Nuclear Magnetic Resonance Detection of Two Distinctly Different Chains in the Orthorhombic Crystalline Phase of Polyethylenes†

Luminita Hillebrand, Angelika Schmidt, Andreas Bolz, Michael Hess, and Wiebren Veeman*

Physikalische Chemie, Gerhard-Mercator-Universität Duisburg, 47048 Duisburg, Germany

Robert J. Meier and Geert van der Velden

DSM Research, P.O. Box 18, 6160 MD Geleen, Netherlands

Received February 11, 1998; Revised Manuscript Received May 15, 1998

ABSTRACT: Several commercial and noncommercial, high- and low-density and ultraoriented polyethylene samples, as well as polyethylene samples with inorganic fillers, have been investigated by inversion−recovery cross-polarization magic angle spinning carbon-13 nuclear magnetic resonance (NMR). In all these samples two types of all-trans chains in *orthorhombic* crystalline domains are detected, which give two overlapping carbon-13 lines with different line widths and different relaxation times. From the NMR relaxation parameters we conclude that one type of the crystalline chains, which composes 60−90% of the crystalline fraction in all samples, can execute at room temperature 180° flips with a frequency in the kilohertz domain. The other crystalline chains are more rigid and probably are found in more perfect structures in which such chain flips do not occur or occur on a much slower time scale. Adding kaoline filler particles to polyethylene enhances the contribution of the more mobile crystalline chains. The presence of the two distinctly different types of crystalline environments is found in all polyethylene samples investigated so far (more than 25 samples).

I. Introduction

Semicrystalline homopolymers have been the subject of many investigations in order to elucidate the morphology and its influence on the physical properties of polymer materials.

Polyethylene (PE) is such a semicrystalline polymer, with important industrial applications as packaging material or highly stretched fibers. Different analytical techniques revealed that the bulk structure contains chain-folded crystalline lamellae, separated by noncrystalline regions.[1] Depending on the thermal and mechanical history, polyethylene can build polymorphic crystals with orthorhombic and monoclinic structures, both with the polymer chains in an all-trans configuration but with different chain packing. During crystallization from the melt, the lamellae can form spherulites, interspaced by amorphous sections.[2−4]

Carbon-13 solid-state nuclear magnetic resonance (NMR) spectroscopy has proved to be a very useful tool in determining the conformation and mobility of chains in crystalline and amorphous domains. High-resolution carbon-13 NMR spectra show distinct lines that can be attributed to ordered (crystalline) and nonordered (amorphous) regions.[5,6] At room temperature, the orthorhombic packing forms the most stable structure and the carbons in this configuration resonate at ca. 33 ppm. Carbons in the amorphous regions, where the local chain conformation fluctuates between trans and gauche states, give rise to a resonance line at ca. 31 ppm. The relaxation behavior of *each* of these two lines is found to be heterogeneous, i.e., more than one relaxation time is needed to fit the relaxation curves. In the case where the polymer also contains monoclinic structures, a second crystalline carbon resonance is found at 34.4 ppm.

Dielectric and mechanical experiments of PE indicate a main-chain motional process, α-relaxation, in the temperature range between room temperature and the melting point. NMR experiments showed that in some polymers with a helical chain structure a twist defect can move through a crystallite, thereby translating the chain by one unit.[7,8] For PE the twist angle is 180°. This screw motion alone cannot be responsible for the α-relaxation process since the lamellae do not change their shape or size. In a viscoelastic experiment, for instance, there is no coupling with the stress field.[3] The α-process in PE results from changes in the amorphous domains, which are induced by the 180° flips and accompanying translation of chains in and from the crystalline phase.[3]

The nature of the boundary between the crystalline and the amorphous phase in polyethylene has been also subject of many investigations. Kitamaru et al.[9] measured three different carbon T_{1C} values for the orthorhombic crystalline phase, which means that this region behaves heterogeneously with respect to motions in the megahertz frequency range. In the same paper Kitamaru et al. detected a downfield shoulder on the amorphous line and assigned it to an *unordered phase* in the interfacial region.

In a recent review Mandelkern[10] concludes from various experiments, such as neutron scattering, Raman spectroscopy, calorimetry, dielectric relaxation, and NMR, that in semicrystalline polymers a less-ordered interphase must exist, situated between the crystalline lamellae, and an amorphous phase above the glass-transition temperature T_g. The evidence for the existence of such an interphase from Raman experiments was, however, thoroughly investigated and subsequently questioned in a paper by Naylor et al.[11]

† We dedicate this work to the 65th birthday of Professor Dr. P. Sartori, Universität Duisburg.

S0024-9297(98)00223-X CCC: $15.00
Published on Web 07/10/1998

Table 1. Preparation Method and Properties of Two Commercial High-Density PE Samples

	HDPE sample 1	HDPE sample 2
preparation method	solution technique	slurry technique
comonomer		C4
density (g/cm^3)	0.963	0.952
lamellar thickness (nm)	18.8	14.8
crystallinity (%)	73.6	65.7
M_w (g/mol)	66 000	73 000
melt index I_2 (g/10 min)	8	10

Wunderlich[12] reported an intermediate phase in polyethylene, whose carbons resonate at the same chemical shift as the crystalline carbons, at 32.9−33.0 ppm; this intermediate region is supposed to involve carbon atoms in the all-trans conformation, sufficiently ordered to generate crystalline peaks in the diffraction patterns.

In this report we describe new solid-state NMR experiments for a more detailed look at the structure of the crystalline phase in PE. Our study differs from previous NMR studies of PE by the application of the inversion−recovery cross-polarization (IRCP) technique.[13,14] We observe that the ^{13}C crystalline resonance of the orthorhombic structures at ca. 33 ppm consists of two clearly distinct components with the *same* chemical shift but different relaxation behavior. We have applied this technique to several commercial and some in-house made PEs, with and without inorganic fillers. In all the PE samples investigated so far (more than 25), even in an ultraoriented fiber, the same two crystalline peaks are detected.

II. Samples and NMR Pulse Sequences

Samples. We have investigated 25 different PEs, synthesized in various ways, with different catalysts and comonomers, which resulted in materials with different molecular mass, density, crystallinity, and composition. Four of these are commercial high-density PE samples with a crystallinity of about 70% (from the density), and prepared either via the solution or the slurry technique, with Ti- or chromium-based catalysts. Three of the samples are copolymers, copolymerized with minor amounts of 1-butene or 1-octene. Since not all samples are as well characterized as these four samples, most of the experimental results reported here, originate from these samples. The parameters of two of these commercial samples, denoted as samples 1−2, are given in Table 1. The samples were compression-molded into plaques of about 2 mm thickness, from which cylindrical disks were cut with a diameter equal to the diameter of the magic angle spinning rotor. These disks were then stacked in the rotor.

Although we do not present the detailed results of the experiments on all 25 samples since the conclusions are basically the same for all samples, we do want to mention that among the other nonfilled PE samples investigated, two were polymerized in solution with a metallocene catalyst and with an octene comonomer (crystallinity 55.4−58% from density). Also, two pressure-extruded ultraoriented PE fibers and some low-density PEs were investigated. One low-density ethylene−octene copolymer is prepared with a Ziegler−Natta catalyst in solution (crystallinity 46−48%) and another one is a very low density PE (VLDPE) by the tube technology (crystallinity 33%).

Polyethylene samples filled with kaoline (particle diameter 2 μm, specific surface area 21 m^2/g, density 2.62 g/cm^3) were prepared via the slurry technique with a homogeneous catalyst based on bis(cyclopentadienyl)-zirconium dichloride/methylaluminoxane in the Max-Planck-Institut für Kohlenforschung (Mülheim, Germany). The filler particles were present during the polymerization. The parameters of the filled PE are listed in Table 2.

Table 2. Properties of PE Samples with Inorganic Fillers

sample	filler content (vol %)	density[a] (g/cm^3)	crystallinity[b]	melting point[b] (K)
PE	0	0.94	59	399
PE/kaoline	5.0	1.01	62	402
	35.4	1.57	56	401

[a] Density was determined by a pycnometer. [b] The crystallinity and melting points were obtained on first heating with a rate of 20 K/min by a Perkin-Elmer DSC.

NMR. The PE samples were investigated on a Bruker ASX-400 spectrometer, operating at 400 MHz for ^{1}H.

All experiments were carried out with magic-angle spinning, using 7 mm double-bearing zirconia rotors and a spinning frequency between 2.5 and 4.5 kHz. The 90° pulse length was either 5 or 6 μs and the recycle delay was 3 s. Pulse programs with bilevel decoupling were used in order to vary the strength of the proton decoupling field from 40 up to 100 kHz. Adamantane was used to optimize the Hartmann−Hahn condition and it also served as external secondary chemical shift reference (38.56 ppm for the methylene resonance relative to TMS). Spectra at different delay times were obtained for all experiments by block-averaging to avoid possible effects of spectrometer drift.

The pulse scheme for the IRCP experiment is given in Figure 1a. The cross-polarization period τ_1 is 500 μs for all experiments reported in this paper. The variable contact time τ_2, during which the proton spin temperature is inverted by a 180° phase shift of the proton spin-lock field, has been varied in the range from 5 to 5000 μs.

The proton spin−lattice relaxation time T_1 is detected with an inversion−recovery experiment via the ^{13}C signals (see Figure 1b).

For the measurement of the proton $T_{1\rho}$ and T_2 relaxation times the standard pulse sequences were combined with the IRCP pulse sequence, as shown in Figure 1c,d. In this case the contact time τ_2 is 22 μs for both experiments. The variable delay time in Figure 1c,d has been varied between 0.5 and 30 ms for the proton $T_{1\rho}$ measurements and between 1 and 40 μs for the proton T_2 experiment.

Carbon T_2 relaxation times are measured by the Hahn spin−echo method combined with IRCP (Figure 1e). This pulse sequence consists of a rotor-synchronized 90°(^{1}H)−IRCP−τ−180°(^{13}C) sequence, followed by detection of the carbon spin−echo after a time 2τ. The contact time τ_2 was 29 μs. The delay τ for the carbon T_2 measurements has been varied from 294 to 13 794 μs. It depends on the period of the rotor rotation T_R, as shown:

$$\tau = nT_R - \pi/2 \qquad (1)$$

where n is an integer.

III. Experimental Section

III.1. Unfilled PE. A. Inversion−Recovery Cross-Polarization Experiments. Figure 2 shows

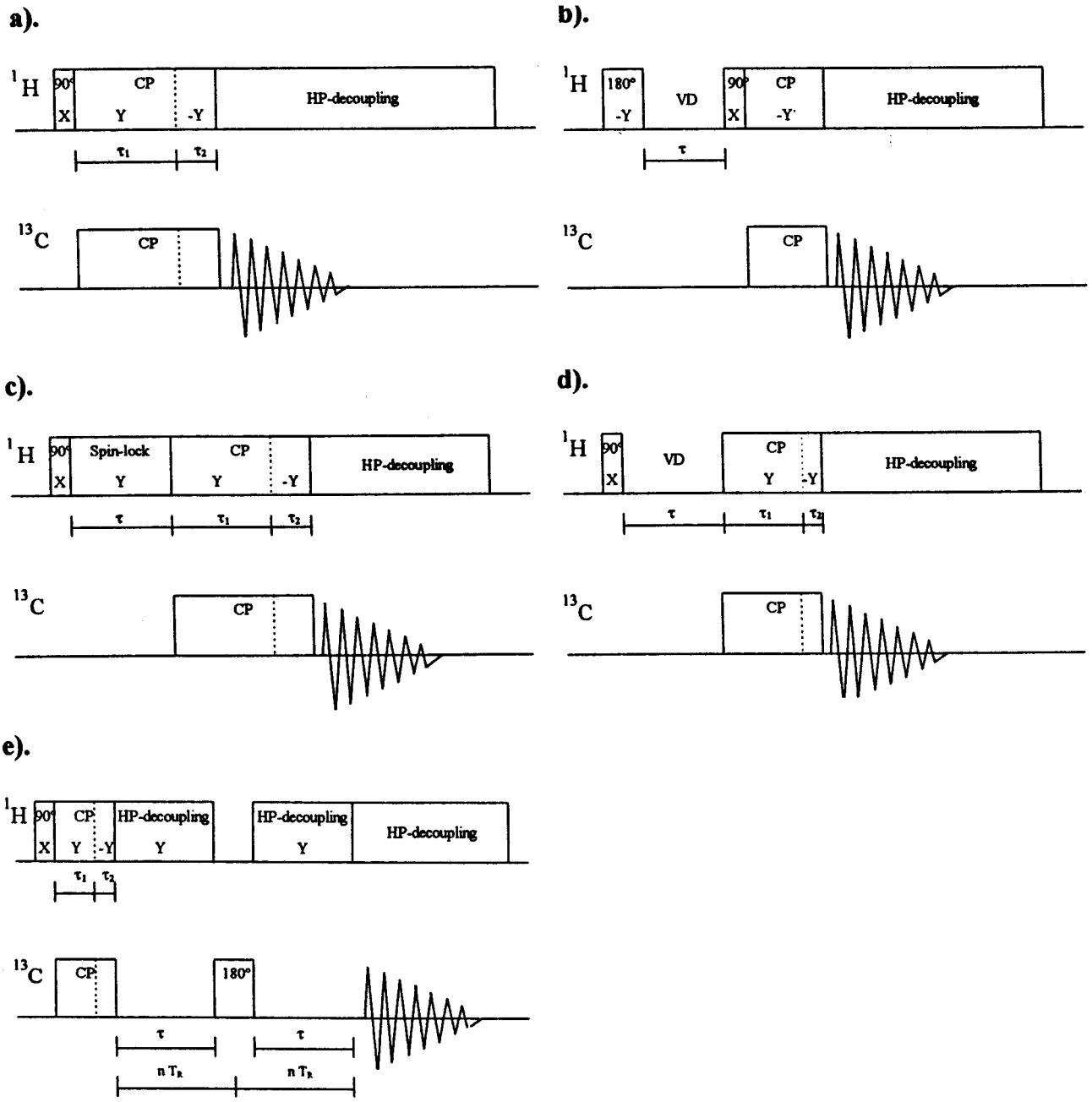

Figure 1. Pulse sequences for the performed experiments: panel a shows the standard IRCP sequence where during τ_2 the phase of the proton spin−lock field is reversed. In panel b the pulse sequence for the proton spin−lattice relaxation experiment is given. Panels c−e show the pulse sequences for the proton T_1, proton T_2, and carbon T_2 relaxation experiments, combined with the IRCP experiment.

the stacked plot of the IRCP experiment, with selected values of the variable contact time τ_2 for HDPE sample 1. The first spectrum, with $\tau_2 = 5$ μs, is comparable to the normal ^{13}C CP-MAS spectrum. As described by Earl and VanderHart,[5] the ^{13}C spectrum shows a resonance at 32.8 ppm from the chains in crystalline domains (in short "crystalline chains") and a peak at 31.0 ppm from chains in amorphous regions (in short "amorphous chains"). Due to the shorter cross-polarization rate T_{CH} of the carbons in the crystalline chains (the amorphous T_{CH} is longer because the carbon−proton dipolar interaction is partly averaged by molecular motions), the crystalline line decreases faster with increasing τ_2 than the amorphous peak and the apparent spectral resolution increases. The spectra with τ_2 in the range of 20−22 μs are of special interest, since this is the range where the crystalline peak is expected to be nulled. However, even with very small increments of τ_2, a spectrum with only the amorphous line cannot be observed. The spectra show two crystalline components with the same chemical shift but different line widths and τ_2 dependence. At, for instance, $\tau_2 = 22$ μs a broad crystalline component (cr-b) has already inverted while a narrow component (cr-n) is still positive.

For each sample it is possible to fit all the IRCP spectra of one data set (34 spectra) with a model of three separate Gauss/Lorentz lines (cr-b and cr-n for the crystalline and am for the amorphous peak) by keeping the chemical shifts, line widths, and the fractional Gauss/Lorentz character constant and by only varying the amplitudes. Deconvolution with only two lines fails, even for spectra with short or long τ_2 values where the existence of a second crystalline component at first sight is not evident. Although deconvolution with three lines

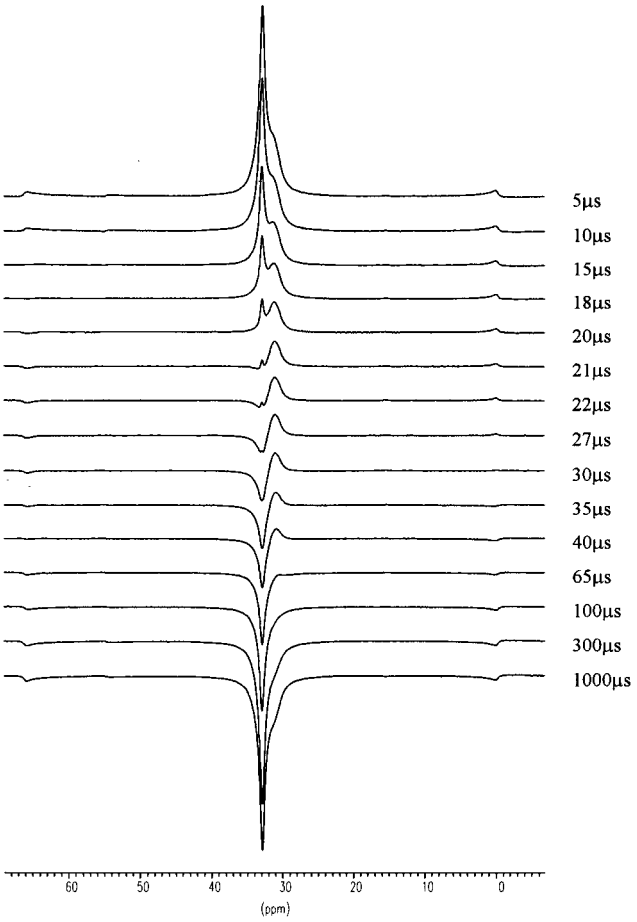

Figure 2. MAS carbon-13 IRCP spectra of HDPE sample 1 as a function of τ_2.

is nearly perfect for the crystalline peak and can be regarded as very accurate, due to the large number of spectra in the IRCP experiment, the fit for the amorphous peak is not completely perfect. Near the nulling point of the amorphous peak we observed a slight upfield shift of its resonance. However, because we intend here to discuss the heterogeneity of the crystalline NMR line, we disregard the small imperfection of the deconvolution of the amorphous line. Figure 3 shows the result of the three-line deconvolution of the IRCP spectra of HDPE sample 1 with $\tau_2 = 5$ μs (Figure 3a) and with $\tau_2 = 22$ μs (Figure 3b). The parameters of the three lines obtained by deconvolution of the IRCP spectra of samples 1 and 2 are given in Table 3. To quantitatively compare the intensity of the two crystalline components cr-b and cr-n, the two crystalline lines from the deconvolution of the IRCP spectrum with $\tau_2 =$ 5 μs have been integrated. Assuming the cross-polarization efficiency of the two crystalline components cr-b and cr-n to be equal, the broad crystalline component cr-b makes up 60−90% of the total crystalline fraction for all samples investigated.

To determine the cross-polarization time constants T_{CH} for each of the three lines, the relative intensities of each component are plotted versus the contact time τ_2 (Figure 4).

When we assume that the T_{CH} time constants are much smaller than the sum of both contact times $\tau_1 + \tau_2$ and that the ^{13}C $T_{1\rho}$ is much longer than T_{CH}, the dependence of the IRCP magnetization, proportional to the ^{13}C intensity, as a function of τ_2 can be described by[13]

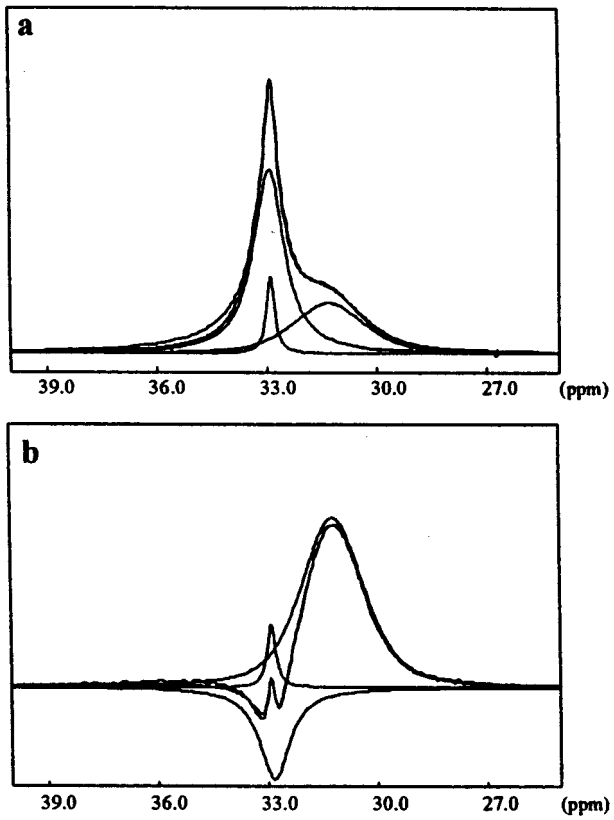

Figure 3. Deconvolution of the IRCP spectra of HDPE sample 1 with $\tau_2 = 5$ (a) and 22 μs (b).

Table 3. Parameters for Each of the Three Gauss/ Lorentz Lines[a]

sample	peak (relative intensity from the spectra with $\tau_2 = 5$ μs)	chemical shift (ppm)	full line width at half-height (Hz)	Gauss character of the Gauss/Lorentz line (%)
1	am	31.10	190	0.50
	cr-n (21%)	32.80	25	1.00
	cr-b (79%)	32.80	85	0.00
2	am	31.1	200	0.50
	cr-n (11%)	32.86	25	0.20
	cr-b (89%)	32.89	96	0.10

[a] Obtained from the three-line deconvolution of the IRCP spectra measured at 9 T; am = amorphous peak, cr-n = narrow crystalline component, and cr-b = broad crystalline component (see also Figure 3).

$$M(\tau_2) = -M_0(1 - 2e^{-\tau_2/T_{CH}})e^{-(\tau_1 + \tau_2)/T_{1\rho}^H} \qquad (2)$$

where M_0 represents the ^{13}C intensity at $\tau_2 = 0$.

It is found that eq 2 gives a very unsatisfactory fit of the IRCP intensities of Figure 4. A much better agreement is obtained with a double-exponential fit according to

$$M(\tau_2) = \{-M_A(1 - 2e^{-\tau_2/T_{CH}^A}) - M_B(1 - 2e^{-\tau_2/T_{CH}^B})\}e^{-(\tau_1 + \tau_2)/T_{1\rho}^H} \qquad (3)$$

The least-squares fit of eq 3 to the data points in Figure 4 is also shown in this figure; the fitting parameters are given in Table 4. The observation of two T_{CH} times, a short and a long value, is not uncommon for samples with relative weak proton dipolar interactions. The long T_{CH} value represents the equilibration process between proton spins near the carbon-13 spins and the proton spin bath.

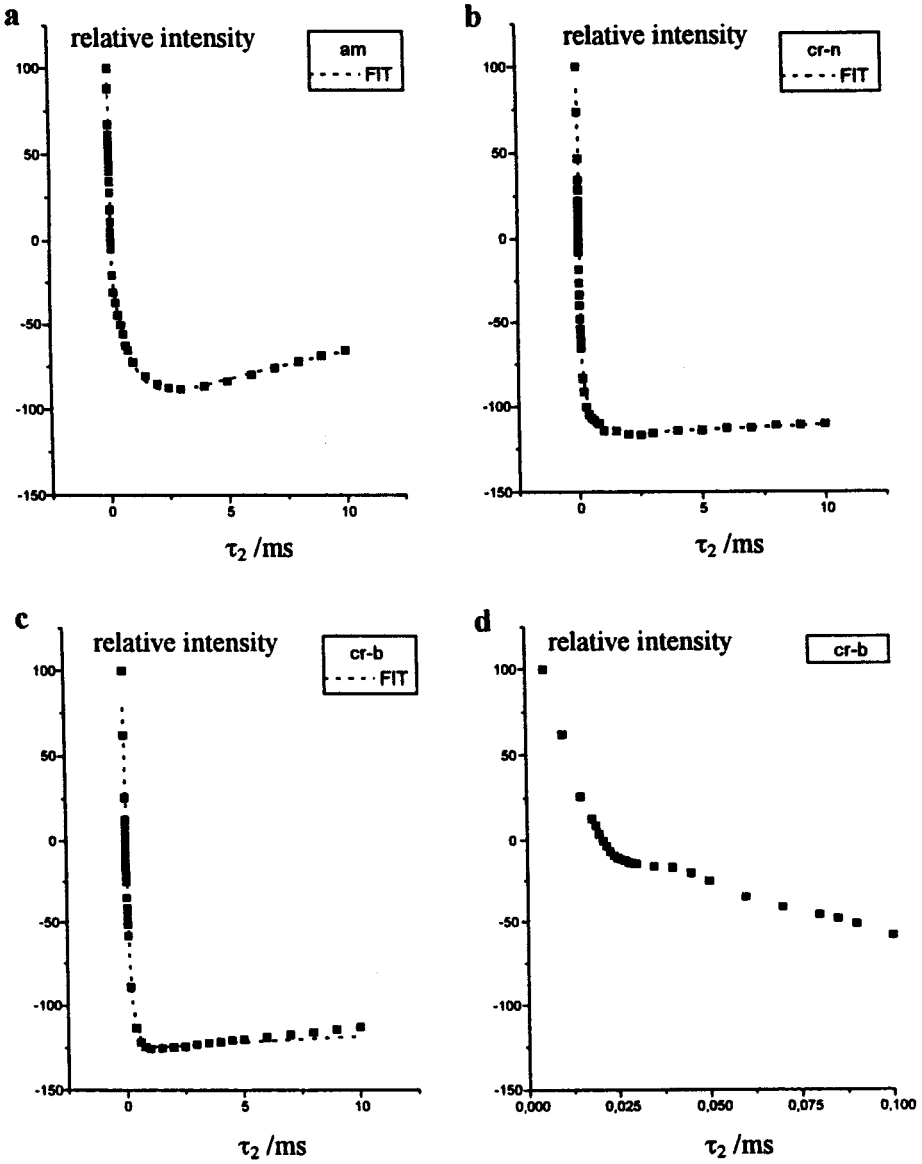

Figure 4. IRCP intensities for the three components after the deconvolution: (a) amorphous, (b) narrow crystalline, and (c) broad crystalline. In panel d the IRCP intensity of the broad crystalline component for short τ_2 values is shown.

Table 4. T_{CH} and ^1H $T_{1\rho}$ Time Constants for Samples 1 and 2 and the Corresponding Fractions from Fitting the IRCP Intensities of the Three Components of Each Sample[a]

sample	peak	T_{CH}^{A} (μs) [fraction (%)][b]	T_{CH}^{B} (μs) [fraction (%)][b]	^1H $T_{1\rho}$ (ms) [fraction (%)][c]
1	am	49 [53]	768 [47]	4.9 [59], 26.5 [41]
	cr-n	26 [71]	261 [29]	92.3
	cr-b	13 [56]	171 [44]	99.8
2	am	57 [62]	960 [38]	3.7 [64], 22.5 [36]
	cr-n	25 [70]	285 [30]	74.2
	cr-b	14 [60]	179 [40]	69.5

[a] $\tau_2 = 22$ μs, MAS = 4500 Hz. [b] ±10%. [c] ±15%.

By expanding the curves of Figure 4c at short τ_2 values for the broad crystalline component cr-b, we find an oscillation of the IRCP intensity as a function of τ_2 (Figure 4d). Surprisingly, only the broad crystalline component cr-b shows this oscillatory behavior and this is observed for all the high-density samples. Such behavior has been reported for systems with relatively isolated C−H pairs.[15] For an isolated C−H spin pair (or an isolated CH_2 group) the cross-polarization process causes an oscillatory exchange of magnetization between the C and H spins. This oscillation is damped by the proton−proton interactions. Therefore, in a strongly coupled proton spin reservoir the cross-polarization buildup curves do not show such oscillatory behavior. Our observation means that for the carbons, responsible for the broad crystalline component, the carbon−proton dipolar interaction is stronger than or at least of the same order of magnitude as the proton−proton dipolar interaction. In a later section we will discuss this aspect further.

To investigate whether the presence of two peaks for the crystalline phase via IRCP is characteristic for other PEs as well, we applied the IRCP method to all PE samples mentioned above. The deconvoluted spectra for all investigated samples show the same feature for the crystalline regions at 32.8 ppm: two peaks with the same chemical shift but different line widths. Some typical examples are shown in Figure 5.

The question whether the two crystalline lines are real and represent two different types of crystalline structures within the orthorhombic phase or are a consequence of a spin dynamics effect of the IRCP experiment will be addressed in the discussion section.

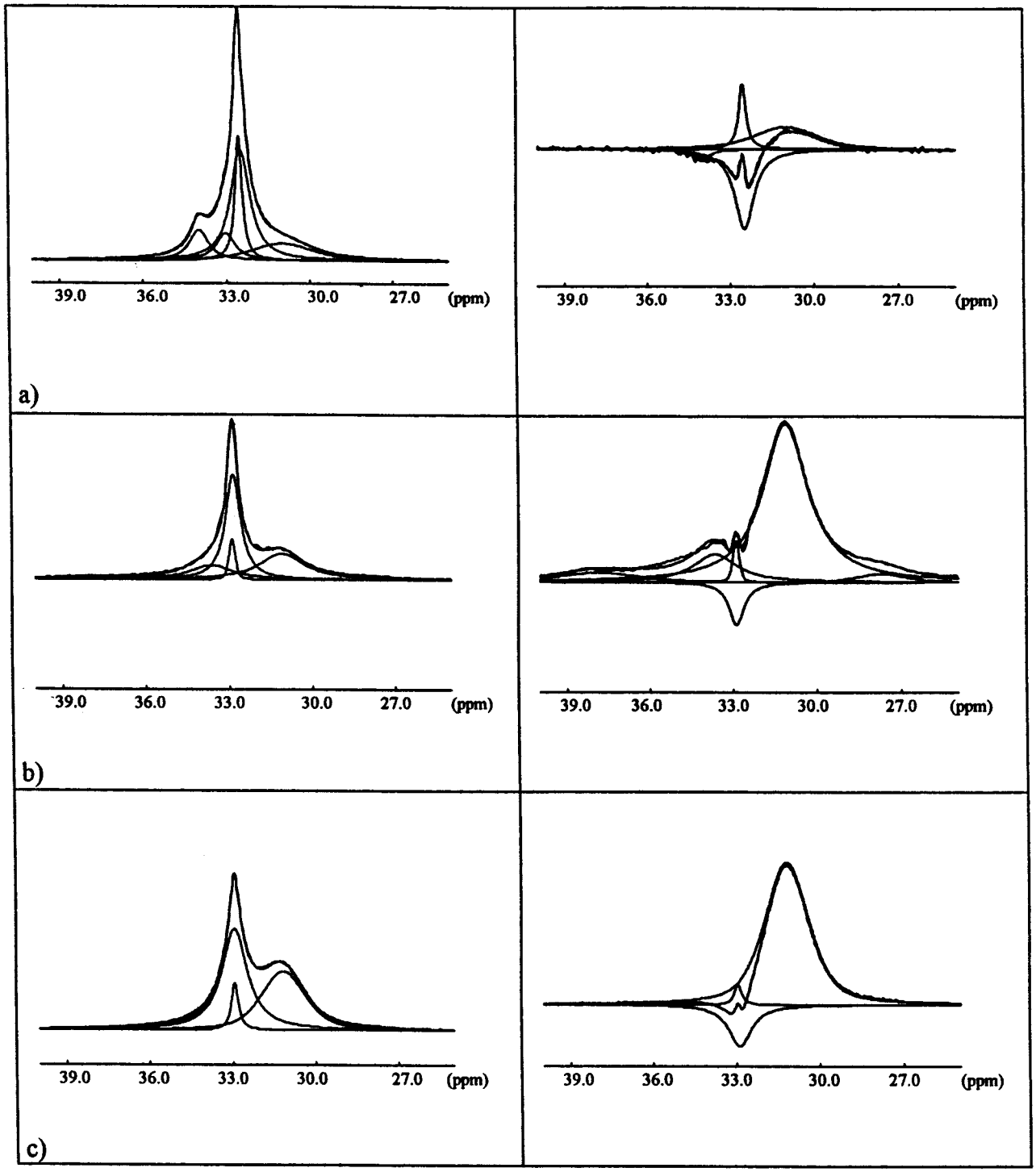

Figure 5. Deconvolution of the IRCP spectra of three different PE samples (at $\tau_2 = 5$ and 22 μs), showing the detection of a cr-n and cr-b peak at 32.8 ppm in the crystalline region for the following: (a) Ultraoriented PE fiber: in addition to the cr-n and cr-b resonance of the orthorhombic crystalline domains, here a third crystalline component is detected at ca. 34 ppm from monoclinic domains and a fourth at ca. 33 ppm, probably from the monoclinic/orthorhombic interface. (b) Low-density polyethylene−octene copolymer, prepared with a Ziegler−Natta catalyst in solution (crystallinity 46−48%). Also here a monoclinic peak is observed and in addition two resonances at ca. 37.5 and 27.3 ppm from side groups. (c) Low-density polyethylene−octene copolymer, polymerized in solution with a metallocene catalyst (crystallinity 55.4−58%)

Since it is known that the carbon line width of PE is strongly dependent on the proton decoupling strength, we show in Figure 6 the dependence of the carbon cr-n and cr-b line width on the proton decoupling strength. It is clear that for decoupling strengths over 70 kHz the cr-n and cr-b line widths become practically independent of the decoupling strength but remain clearly different.

Up to 90 °C both crystalline lines are present, but above 90 °C the narrow line cr-n is absent and only the broad line cr-b remains (Figure 7). The line width of the cr-n line increases minimally with temperature; the line width of cr-b, however, increases from 75 Hz at room temperature to 150 Hz at 100 °C (with 60 kHz proton decoupling strength). Above 60 °C two lines with different chemical shifts and line widths are needed to fit the amorphous line. They are attributed to noncrystalline, liquidlike domains and more rigid amorphous domains.

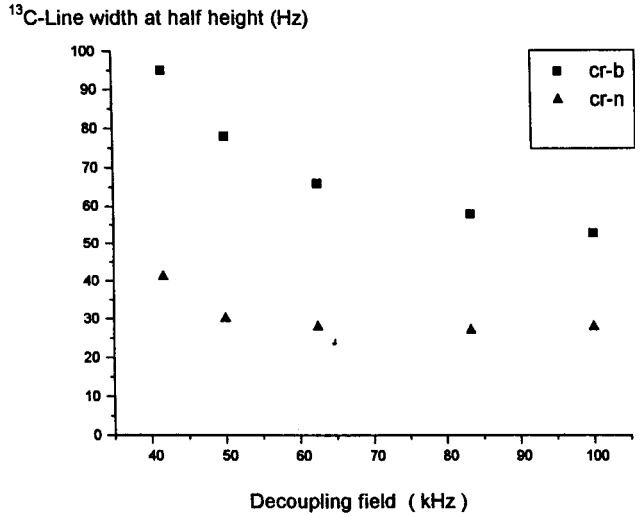

Figure 6. Line width of the cr-b and cr-n ^{13}C NMR line of sample 1 as a function of the decoupling field in kilohertz.

In Figure 8 the IRCP spectra are shown of sample 1 after annealing for 2 weeks at 130 °C followed by an extraction treatment with HNO_3. This treatment has completely removed the amorphous domains, but clearly both the narrow and broad crystalline components are still there.

B. Inversion−Recovery Proton Spin−Lattice Relaxation Experiments. Another inversion−recovery method, different from the one discussed above, is the standard method to determine the spin−lattice relaxation time T_1 (the 180−τ−90 method) (Figure 1b). After inversion of the proton magnetization, the z-magnetization relaxes during τ and is then observed via the carbon signal. Also here the signal passes a null value and components with small differences in ^{1}H T_1 should manifest themselves around this nulling point. Therefore, the delay time has been varied between 0.5 and 0.9 s and, as expected, near the nulling point of the crystalline phase, we notice two lines that invert one after the other at slightly different delay times (Figure 9a). Deconvolution of the spectra (Figure 9b) confirms the results of the IRCP experiment and shows two peaks for the crystalline region, with different line widths [$\nu_{1/2}$(cr n) = 31−38 Hz and $\nu_{1/2}$(cr b) = 66−68 Hz], but almost identical chemical shifts (32.8−32.9 ppm). Although, as we will show in the next section, there is rather efficient spin diffusion within the crystalline parts of the sample, the spin diffusion is not so fast that the longitudinal proton relaxation times of both crystalline components are exactly equal. By the nulling method, however, differences of a few milliseconds can be detected.

C. Inversion−Recovery Cross-Polarization Combined with ^{1}H $T_{1\rho}$ Determination. The relation between nuclear spin relaxation times and the molecular motional frequencies makes relaxation time measurements attractive for the characterization of polymers. However, as already mentioned above, relaxation times can also provide information about spin diffusion effects and, since spin diffusion depends on spatial distances between groups of spins, about average distances between domains in heterogeneous solids.[16] Above we saw that the proton T_1 values of the domains responsible for the narrow and broad crystalline carbon resonance are very close. This suggests that on the time scale of about 1 s spin diffusion is fast enough to almost equalize the two proton relaxation times. To see how efficient the spin diffusion is, we also determined the proton $T_{1\rho}$ values via the carbon signals. The combination of the proton $T_{1\rho}$ experiment with the IRCP pulse sequence (Figure 1c) leads, for a constant τ_2 value, to a series of ^{13}C spectra with each line intensity modulated by the proton $T_{1\rho}$ relaxation. By taking τ_2 = 22 s we ensured that each carbon spectrum could be accurately deconvoluted into the three component lines discussed above and that for each component line we could determine the corresponding proton $T_{1\rho}$. The proton relaxation decay of both crystalline peaks can be fitted well with a monoexponential decay, and the amorphous line with a biexponential function. Table 4 summarizes the proton $T_{1\rho}$ values obtained in this way for the amorphous (am) protons, for the protons related to the narrow crystalline line (cr n), and for the protons related to the broad crystalline line (cr b).

The proton $T_{1\rho}$ values of the cr-b and cr-n lines are close for each sample, just as in the case of the proton T_1 experiments, but they differ from those of the amorphous phase. Both the proton T_1 and the $T_{1\rho}$ experiments suggest efficient spin diffusion between the protons in the crystalline domains that are responsible for the cr-n and cr-b resonances. This implies that the two types of structures (cr-b and cr-n) are spatially closer than about 1 nm.[16] Two nonequal proton relaxation times for the amorphous phase point out the existence of at least two, spatially separated, amorphous domains, with different proton mobilities.

At higher temperatures, the proton $T_{1\rho}$ values of the cr-b and cr-n lines decrease but remain approximately equal. At 80 °C the two relaxation times are 4 and 3.1 ms, respectively, for HDPE sample 1. At 100 °C, where only the cr-b line is found, the proton $T_{1\rho}$ value for this sample is 1 ms.

D. Carbon Spin−Spin Relaxation Measurements Combined with IRCP. Since the two detected crystalline carbon lines have different line widths, it is worthwhile to determine the ^{13}C T_2 in order to get information regarding the source of the line broadening. The spectra obtained with the carbon spin−echo IRCP method (Figure 1e) have been deconvoluted with three lines (cr-n, cr-b, and am), with constant chemical shift and line width for cr-n and cr-b and variable chemical shift and line width for am. The relative intensities determined by the integration of each of the components have been plotted versus 2τ. The relaxation data points of sample 1 and its decay curves are shown in Figure 10. All curves for the amorphous domains have been fitted monoexponentially. The ^{13}C T_2 relaxation times of the two HDPE samples, together with the calculated and experimental ^{13}C line widths, are given in Table 5.

III.2. PE Filled with Inorganic Particles. The same IRCP experiments as discussed above have been applied to PE, filled with varying amounts of particles of the aluminosilicate kaoline. These polymers have been polymerized in the presence of the filler. The spectra have been deconvoluted as described above and again show for all samples, except PE with 35% kaoline, two crystalline carbon lines at about 33 ppm. The NMR parameters are given in Table 6. An important result here is the fact that the relative intensity of the cr-b line increases with the amount of filler. With 35% filler only the a-b line can be detected.

Unlike the case of the unfilled PEs, for the filled PE the $T_{1\rho}$ values of the protons corresponding to the cr-n

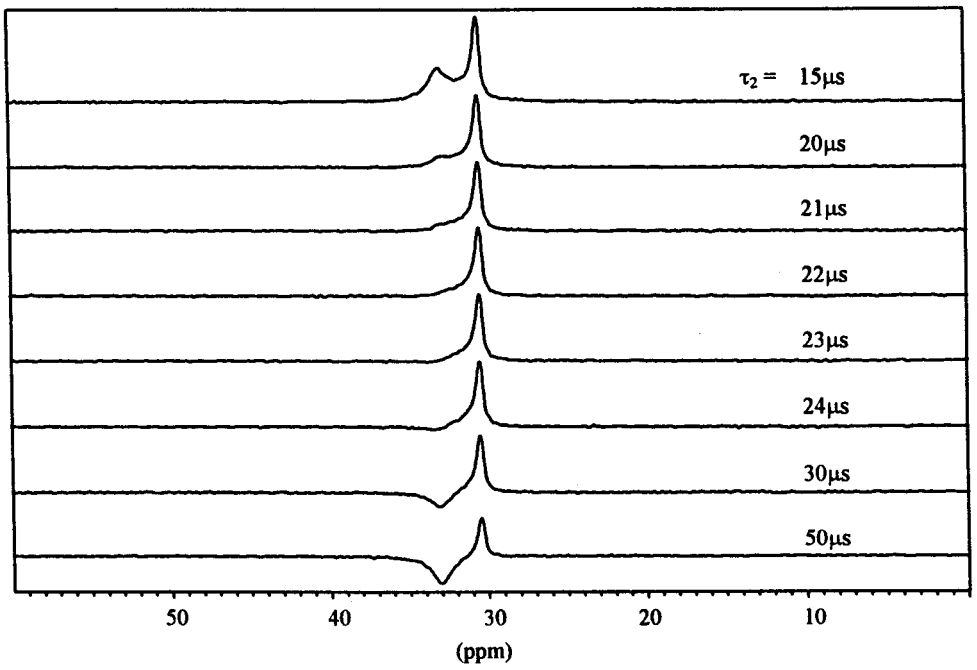

Figure 7. IRCP spectra of sample 1 at 100 °C.

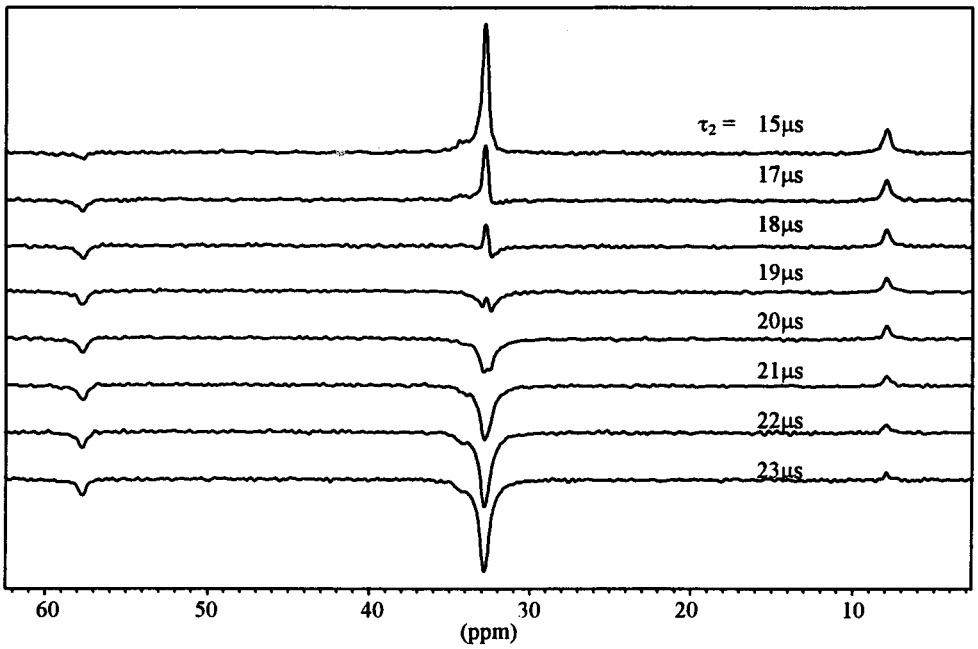

Figure 8. IRCP spectra of sample 1 after annealing for 2 weeks at 130 °C and followed by HNO_3 extraction treatment.

and the cr-b domains are no longer equal. The proton $T_{1\rho}$ corresponding to the cr-b carbon line decreases significantly with increasing amount of filler for all fillers and approaches the value for the amorphous protons.

IV. Discussion

The results of the previous section unambiguously show for both high-density and low-density PE, filled and unfilled, the presence of two overlapping resonances at 32.7−32.9 ppm with different line widths, different cross-polarization rates, and also very slightly different proton T_1 values. By now, ca. 25 PE samples have been investigated and all samples show these two lines. Some representative examples are shown in Figure 5. Both resonances are found at a chemical shift that corresponds to the orthorhombic crystalline structure. The carbon resonance of a monoclinic structure should occur at 34.4 ppm and, by melting the sample and quickly cooling, this structure can indeed be induced in our PE, however, without affecting the two overlapping resonances at 32.7−32−9 ppm. The spectra of the extracted PE in Figure 8 show that acid treatment removes the amorphous domains but that both the cr-n and cr-b components remain.

For a long time, our main worry has been that the two lines cr-n and cr-b could result either from a spin dynamics effect inherent to the IRCP experiment (the spin system may not be in equilibrium after the short τ_2 and unwanted coherences may contribute) or from the anisotropy of the CP rate.

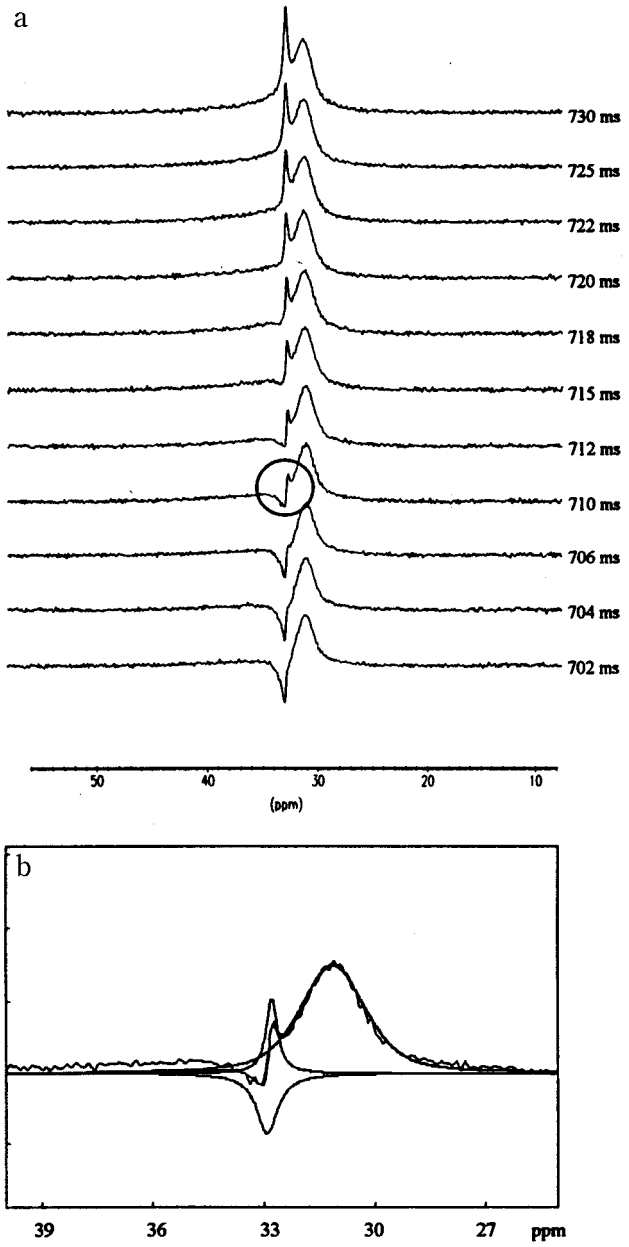

Figure 9. (a) ^{13}C CP-MAS-detected relaxation spectra of sample 1 according to the pulse sequence of Figure 1b. (b) Deconvolution with three lines of the relaxation spectrum with 710 ms.

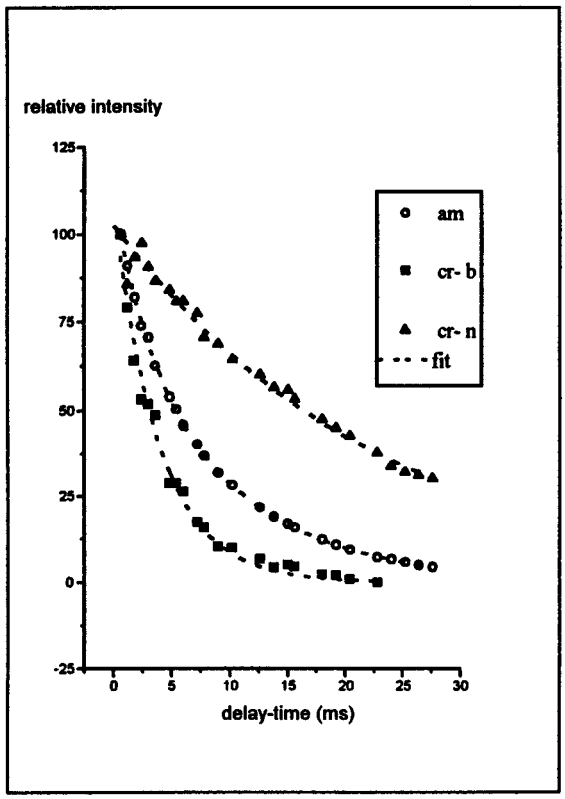

Figure 10. ^{13}C IRCP CP-MAS-detected carbon T_2 decay of the three resonances cr-n, cr-b, and am for sample 1.

Table 5. Carbon-13 T_2 Relaxation Times, Corresponding Homogeneous Line Width at Half Height ($\nu_{1/2}$*), and Experimental Line Width at Half Height [$\nu_{1/2}$ (exp)][a]

sample	^{13}C line	T_2^C (ms)[b]	$\nu_{1/2}^* = 1/\pi T_2^C$ (Hz)[b]	$\nu_{1/2}$ (exp) (Hz)[c,d]
1	am	10.1	32	175
	cr-n	22.1	14	31
	cr-b	3.7	86	71
2	am	9.7	33	187
	cr-n	22.7	14	25
	cr-b	3.9	82	91

[a] From the carbon spin−echo experiment with IRCP (MAS = 3500 Hz) at room temperature. [b] ±15%. [c] ±10 Hz. [d] The line width data in this column are not exactly equal to those given in Table 3 because they are determined by independent, different experiments. The data in Table 3 come from an IRCP experiment; the data in this table are from an IRCP/^{13}C T_2 experiment.

We believe we have three arguments to show that the observed effects are not caused by a spin dynamics effect due to the IRCP experiment and that our observations imply that two types of orthorhombic crystalline PE chains exist in all PEs:

(i) The same two lines, cr-b and cr-n, also appear in the proton spin−lattice inversion−recovery experiment at about the delay time where the magnetization is nulled (see section III.1B).

(ii) The experiments on the filled PE sample clearly show that the intensity of the broad crystalline component cr-b increases with increasing filler content. If the presence of the two orthorhombic resonances would be done to an anisotropic CP rate (see (iii) below), it would be impossible to understand why the presence of filler particles would affect the CP anisotropy. The presence of the filler particles apparently favors a similar structure as that responsible for the cr-b line. The filler particles may act as nucleation centers during the crystallization process. The fact that the proton $T_{1\rho}$ decay of the cr-b line in the PE filled with 35% kaoline becomes biexponential suggests that there are two different types of cr-b chains. One type is formed by the cr-b chains that are already present in the unfilled PE's, with a proton $T_{1\rho}$ equal to that of the cr-n carbons. The second type is induced by the filler particles and nearer to the amorphous domains, therefore their proton $T_{1\rho}$ is near to that of the amorphous protons.

(iii) The CP rate is anisotropic, and in samples without an overall orientation this must lead to a distribution of CP rates. The distribution of cross-polarization rates could be doubly peaked. This would lead to similar experimental observations as reported here. The two different lines would then result from the same crystalline structure but originate from PE fragments with different orientations relative to the external magnetic field. Since the line width may also

Table 6. Experimental NMR Parameters of Kaoline-Filled PEs

sample	filler fraction (vol %)	^{13}C line	chemical shift (ppm)	crystalline fraction (%)	line width (Hz)	^{1}H $T_{1\rho}$ (ms) [fraction (%)]
PE	0	am	30.9		141	4.1 [57%], 21.6 [53%]
		cr-n	32.7	33	30	225
		cr-b	32.7	67	64	173.6
PE//kaoline	5.0	am	30.9		156	5.0 [53%], 20.1 [47%]
		cr-n	32.7	21	30	209
		cr-b	32.7	79	64	209 [80%], 1.9 [20%]
PE/kaoline	35.4	am	30.8		243	6.2 [79%], 25 [21%]
		cr-b	32.6	100	81	4.1 [41%], 215 [59%]

be anisotropic, this would then also explain the difference in carbon line width. Experimentally we proved that this presumption is not correct by performing the experiment under slow magic-angle spinning (1000 Hz). As expected, the relatively strong-spinning side bands (SSB) at the low MAS rate invert at different times in the IRCP experiment, since different molecular orientations with different CP rates contribute unequally to different SSBs. Therefore, each SSB emphasizes certain selected orientations and if the two crystalline carbon lines cr-n and cr-b resulted from differently oriented molecular fragments, not all the SSBs in the IRCP experiment should show these two lines with the same ratio. This is, however, not the case: the experiment shows that near the nulling point each SSB consists of the two crystalline lines, exactly as for the center band.

The possibility that a bimodal distribution of cross-polarization rates is responsible for the two crystalline lines can also be excluded by calculating the orientation dependence of the CP rate for the PE orthorhombic structure. It turns out (see the Appendix) that although the CP rate is anisotropic, the rates do not show a clear bimodal distribution.

From these three arguments we conclude that in all PE samples investigated, two types of chains in the orthorhombic crystalline structure exist, both with an all-trans chain conformation. One type is responsible for the cr-b ^{13}C line; the other, for the cr-n ^{13}C line. The chemical shifts of both lines are equal, but they differ in the following NMR properties: (a) Line width: The narrow cr-n line is inhomogeneously broadened [$\nu_{1/2}$(exp) > $\nu_{1/2}'$], but the broad cr-b line is practically completely homogeneously broadened [$\nu_{1/2}$(exp) ≈ $\nu_{1/2}'$] (see Tables 3 and 5). (b) CP rate: The cr-b line has a shorter T_{CH} than the cr-n line (Table 4). (c) CP oscillations: The cr-b line shows a small CP oscillation (Figure 4d). (d) Proton T_2: A proton T_2 experiment showed that the protons near cr-b carbons have a shorter T_2 (5 μs) than the protons near the cr-n carbons (7−12 μs).

Since during the free induction decay or the spin−echo experiment all dipolar interactions that involve carbon spins are eliminated by MAS and proton decoupling, the only source for the homogeneous broadening of the cr-b line is molecular reorientations with frequencies of the order of the MAS frequency (2−4 kHz) and/or of the proton decoupling field (up to 100 kHz).

Likely molecular motions to consider are polymer chain flips over 180°. As discussed in the Introduction these helical jumps are responsible for the α-relaxation and chain diffusion from the crystalline into the amorphous domains,[6,7] although at somewhat higher temperatures than room temperature. We first want to show that exactly such motions can also explain our observations a−d and then discuss why so far these motions have escaped detection at room temperature.

It is clear that when we could consider the CH_2 group as one isolated spin system, the CP curve would show oscillations. The dipolar coupling to protons in other CH_2 groups damp such oscillations. Therefore we compare the distances between protons in the same chain and between protons in different chains. Using the interatomic distances of orthorhomic PE,[17] we find for the nearest distance between protons of neighboring CH_2 groups in an *all-trans*-PE chain 2.358 Å, corresponding[8] to a dipolar interaction of 9 kHz. The nearest distance between protons of neighboring chains is 2.724 Å, corresponding to 6 kHz dipolar interaction. By comparing these inter-CH_2-group proton−proton dipolar interactions to the intragroup ^{13}C−^{1}H dipolar interaction of 23 kHz, we conclude that the condition for oscillations in the CP curve (^{13}C−^{1}H dipolar interaction > ^{1}H−^{1}H dipolar interactions) seems to be fulfilled[15] and that only because of the many proton−proton interactions are the PE CP curves not all oscillatory. For rigid chains the interchain + intrachain ^{1}H−^{1}H dipolar interactions apparently make the proton−proton spin flip-flops fast enough to prevent CP oscillations. Consequently, the cr-n NMR lines must result from rigid chains. PE chain 180° flips faster than ≈10 kHz eliminate the *inter*chain ^{1}H−^{1}H dipolar interactions and thereby *strengthen* the ^{13}C−^{1}H dipolar interaction within a $^{13}CH_2$ group. In general, the proton flip-flops in a strongly coupled proton system reduce the ^{13}C−^{1}H dipolar interaction, because the ^{1}H spin in the ^{13}C−^{1}H pair is randomly modulated by the flip-flops with neighboring proton spins (self-decoupling[18,19]). A decrease of the proton flip-flop rate can occur in PE domains where the *inter*chain ^{1}H−^{1}H dipolar interactions are averaged out by 180° polymer chain flips. For chains that can execute such flips, this leads to (a) stronger ^{13}C−^{1}H dipolar interactions within a $^{13}CH_2$ group and thus a faster CP rate and (b) CP oscillations. For the same reason, chain flips also increase the ^{1}H−^{1}H dipolar interaction within a $^{13}CH_2$ group and this leads to a shorter T_2 for protons.

Normally, increased molecular motions reduce the ^{13}C−^{1}H CP rate by partly averaging the ^{13}C−^{1}H dipolar interaction. This is not the case here, while a 180° flip of a chain fragment does not affect the intragroup ^{13}C−^{1}H or ^{1}H−^{1}H dipolar interactions. Therefore, our NMR observations can be explained by 180° flips of the PE chains and *only such motions* can explain our observations a−d, mentioned above.

To explain our experimental results we propose that the cr-b carbons are found in all-trans orthorhombic crystalline PE chains that contain twist defects, which cause flips of the chains over 180° with a frequency over ∼10 kHz. The cr-n resonance results from chains that do not make such flips or make them only at an appreciably lower rate.

To see why these 180° chain flips, frequent even at room temperature, have escaped detection so far, or in other words, how it comes that these motions do not contribute to the α-transition, it should be realized that

180° chain flips alone cannot be detected directly, since a crystalline lamella before and after the flip of one or more chains is indistinguishable in terms of NMR, viscoelastic, or dielectric experiments. Such flips are observable only when the flip and the accompanying translation over one chain unit is followed by additional flips and translations of the same chain in the same direction. The ultimate effect of consecutive chain translation is a transport of chains from the crystalline regions into the amorphous domains or vice versa. This chain diffusion can be detected by two-dimensional exchange NMR,[8] while in the process the carbon chemical shift changes from the crystalline value (≈33 ppm) to the amorphous value of ≈31 ppm or vice versa, and by mechanical or dielectric experiments, while parts of the chain that extend into the amorphous domains above and below the lamellae must change their lengths.

A simple explanation for the fact that the frequent 180° flips, which we detect even at room temperature, have not been observed before could be that the motion does not result in a displacement of a chain but is a sequence of flips and translations in opposite directions. Such a situation would arise when the defect that travels through the chains is bounced at the surfaces of the lamellae, because at room temperature, the activation energy to displace the chain over more than one unit into the amorphous phase is too high (105 kJ/mol[3,8]). Only indirect NMR parameters, like the line width or relaxation times, can probe such motions, as shown by our experiments.

Therefore, our experimental results can be explained by assuming that the crystalline lamellae in PE consist of chains with twist defects locked in a certain chain length, able to travel through the chain length back and forth, thereby each time rotating the flat zigzag PE chains over 180° in opposite directions. These chains, by modulating the various spin interactions as described above, generate the cr-b carbon lines. Other chains would either not have such defects or the motion of the defect would be heavily constrained.

The relative decrease of the intensity of the cr-n resonance with increasing density of kaoline filler particles suggests that the chains responsible for the cr-n line are located in more perfect crystallites without the twist defect.

It is of interest to speculate about where the two types of chains are to be localized. The two types of chains could coexist in one lamella, as suggested by the proton spin−lattice relaxation results of the unfilled PE. One type of chains could correspond to the chains that re-enter the same lamella at a neighboring site, the other type, to chains that do not re-enter the same lamella. On the other hand, the similarity in spin−lattice relaxation times may be accidental and the two types of chains could be located in different lamella. It is known for PE, and many other polymers, that, after completion of the primary crystallization at a certain temperature below the melting temperature, crystallization has not come to an end but continues at a lower temperature.[3] This secondary crystallization produces additional crystallites, which may have more or less defects than the crystallites arising from the primary crystallization process. More work is needed to investigate these aspects.

V. Conclusion

Our experiments show that in PE (independent of the polymer density) two different types of chains in the orthorhombic crystalline phase exist, both in an all-trans configuration. They are responsible for two overlapping resonances in the ^{13}C IRCP-MAS spectrum with different line widths: a broad line cr-b and a narrow line cr-n.

All our experimental observations can be explained by assuming that the chains responsible for the cr-b carbon resonance, which form the main fraction of the crystalline domains, make already at room temperature relatively fast (kilohertz regime) 180° chain flips by a travelling chain twist defect. The motion of the defect must be limited in the sense that no significant displacement of PE chains results from it. The chains responsible for the cr-n carbon resonance do not show these motions or show them only on a much longer time scale and probably are found in more perfect crystalline structures. The filler particles in PE enhance the mobile, imperfect crystalline fraction.

The presence of the two distinctly different types of crystalline environments seems to be a universal feature of semicrystalline PE since the two types have been detected in 25 different PEs.

Acknowledgment. We thank Professor Fink (MPI für Kohlenforschung, Mülheim) for giving the opportunity and support for the synthesis of the filled PE samples and Dipl.-Ing. M. Zähres and U. Bachorski for their skilled help during the experiments.

Appendix

For a CH_2 spin system the dependence of the cross-polarization rate on the orientation of the CH_2 group relative to the B_0 field can be calculated (where I = ^1H and S = ^{13}C):[20]

$$T_{IS}^{-1} = \frac{1}{2}\sin^2\varphi_S \sin^2\varphi_I M_{2,SI} J_X(\Delta\omega_{eff}) \qquad (1)$$

where

$$M_{2,SI} = \frac{1}{3}\gamma_I^2\gamma_s^2\hbar^2 I(I+1)\sum_{I,S}(1 - 3\cos^2\varphi_{IS})^2 r^{-6}_{IS} \qquad (2)$$

We assume that the anisotropy of the cross-polarization rate mainly depends on the term $\sum_{IS}(1 - 3\cos^2\varphi_{IS})^2 r^{-6}_{IS}$. Then

$$T_{IS}^{-1} \propto \sum_{IS}(1 - 3\cos^2\varphi_{IS})^2 \qquad (3)$$

where θ_{IS} is the angle between the C−H vector and B_0.

We now describe the orientation of the two C−H vectors of a CH_2 group in *all-trans*-PE in an axis system x', y', z', where z' is parallel to the chain axis and the two C−H vectors lie in the x', y' plane, so that the y' axis divides the H−C−H angle into two equal angles of 53.5° each. The length of the C−H vector is not important here and therefore we can assume that $|\vec{C}\,H| = 1$. Then in x', y', z' the two CH vectors are represented by the vectors:

$$CH_1 = \begin{pmatrix}\sin 53.5\\ \cos 53.5\\ 0\end{pmatrix} \quad \text{and} \quad CH_2 = \begin{pmatrix}-\sin 53.5\\ \cos 53.5\\ 0\end{pmatrix} \qquad (4)$$

By rotating the x', y', z' axis system to an x, y, z axis system, in which $z//B_0$, with the Euler angles α, β, γ and

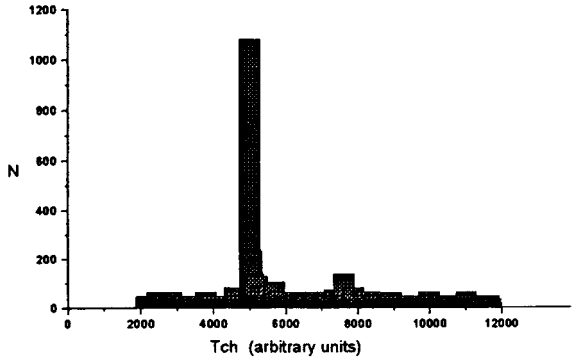

Figure 11. Distribution of cross-polarization times T_{CH} for the CH_2 groups of polycrystalline PE (see Appendix).

rotation matrix R, we find the orientation of the two C−H vectors in the x, y, z frame:

$$R\begin{pmatrix}\sin 53.5\\ \cos 53.5\\ 0\end{pmatrix} = R\begin{pmatrix}0.804\\ 0.595\\ 0\end{pmatrix} = \begin{pmatrix}a_{11}\\ a_{21}\\ a_{31}\end{pmatrix} \quad (5)$$

$$R\begin{pmatrix}-\sin 53.5\\ \cos 53.5\\ 0\end{pmatrix} = R\begin{pmatrix}-0.804\\ 0.595\\ 0\end{pmatrix} = \begin{pmatrix}b_{11}\\ b_{21}\\ b_{31}\end{pmatrix} \quad (6)$$

where[21]

$$R = \begin{pmatrix}\cos\gamma & \sin\gamma & 0\\ -\sin\gamma & \cos\gamma & 0\\ 0 & 0 & 1\end{pmatrix}\begin{pmatrix}\cos\beta & 0 & -\sin\beta\\ 0 & 1 & 0\\ \sin\beta & 0 & \cos\beta\end{pmatrix} \times \begin{pmatrix}\cos\alpha & \sin\alpha & 0\\ -\sin\alpha & \cos\alpha & 0\\ 0 & 0 & 1\end{pmatrix}$$

With $|\vec{C}H| = 1$, the cos φ_1 and cos φ_2 terms can be calculated:

$$\cos\varphi_1 = (\vec{z}\cdot\vec{C}H_1) = a_{31} \quad \text{and} \quad \cos\varphi_2 = (\vec{z}\cdot\vec{C}H_2) = b_{31} \quad (7)$$

As expected, cos φ_1 and cos φ_2 depend only on the angles α and β. The cross-polarization rate can now be calculated, by applying eq 3:

$$T^{-1}_{CH} \propto 2 - 7.752\sin^2\beta\cos^2\alpha - 4.248\sin^2\beta\sin^2\alpha + 7.521\sin^4\beta\cos^4\alpha + 24.716\sin^4\beta\cos^2\alpha\sin^2\alpha + 2.256\sin^4\beta\sin^4\alpha \quad (8)$$

A Fortran program has been used to vary the angles α and β (from 1° to 360°, in 1° steps) and for each α and β the T_{CH} time has been determined and collected in the histogram presented in Figure 11. The T_{CH} values show a wide distribution and even two peaks, but the difference in integrated intensity of these two peaks is so large that we can safely exclude the possibility that the two carbon lines detected in the IRCP experiment are due to an anisotropy of the CP rate.

References and Notes

(1) Kroschwitz, J. I. *Polymers: Polymer Characterization and Analysis*; John Wiley & Sons: New York, 1990.
(2) Billmeyer, F. W. *Textbook of Polymer Science*; John Wiley & Sons: New York, 1984.
(3) Strobl, G. *The Physics of Polymers*; Springer: Berlin, 1996.
(4) Mandelkern, L. *An Introduction to Macromolecules*, 2nd ed.; Springer: New York, 1983.
(5) Earl, W. L.; VanderHart, D. L. *Macromolecules* **1979**, *12*, 762.
(6) Cholli, A. L.; Ritchey, W. M.; Koenig, J. L.; Veeman, W. S. *Spectrosc. Lett.* **1988**, *21*, 519.
(7) Kentgens, A. P. M.; de Boer, E.; Veeman, W. S. *J. Chem. Phys.* **1987**, *87*, 6859.
(8) Schmidt-Rohr, K.; Spiess, H. W. *Multidimensional solid-state NMR and Polymers*; Academic Press: London, 1994.
(9) Kitamaru, R.; Horii, F.; Murayama, K. *Macromolecules* **1986**, *19*, 636.
(10) Mandelkern, L. *Acc. Chem. Res.* **1990**, *23*, 380. Mandelkern, L. *Chemtracts: Makromol. Chem.* **1992**, *3*, 347.
(11) Naylor, C. C.; Meier, R. J.; Kip, B. J.; Williams, K. P. J.; Mason, S. M.; Conroy, N; Gerrard, D. L. *Macromolecules* **1995**, *28*, 2969.
(12) Cheng, J.; Fone, M.; Reddy, V. N.; Schwartz, K. B.; Fisher, H. P.; Wunderlich, B. *J. Polym. Sci., Part B: Polym. Phys.* **1994**, *32*, 2683.
(13) Cory, D. G.; Ritchey, W. M. *Macromolecules* **1989**, *22*, 1611. Cory, D. G.; Shieh, Y. T.; Ritchey, W. M. *Bruker Rep.* **1988**, *2*, 16.
(14) Melchior, M. T. 22nd Experimental NMR Conference, Asilomar, CA, 1990. Wu, X.; Zilm, K. W. *J. Magn. Reson.* **1993**, *A102*, 205.
(15) Müller, L.; Kumar, A.; Baumann, T.; Ernst, R. R. *Phys. Rev. Lett.* **1974**, *32*, 1402. Naito, A.; McDowell, C. A. *J. Chem. Phys.* **1986**, *84*, 4181. Wu, X.; Zhang, S. *Chem. Phys. Lett.* **1989**, *156*, 79. Walther, K. L.; Wokaun, A.; Handy, B. E.; Baiker, A. *J. Non-Cryst. Solids* **1991**, *134*, 47.
(16) Veeman, W. S.; Maas, W. E. J. R. In: *NMR, Basic Principles and Progress*; Diehl, P., Fluck, E., Günther, H., Kosfeld, R., Seelig, J., Eds.; Springer-Verlag: Berlin, Germany, 1994, Vol. 32, p 127.
(17) Wunderlich, B. *Macromolecular Physics*; Academic Press: New York and London, 1973; Volume I.
(18) Abragam, A. *The principles of nuclear magnetism*; Oxford University Press: Oxford, England, 1961.
(19) Haeberlen, U. *High-resolution NMR in solids, selective averaging*; Academic Press: New York, 1976.
(20) Mehring, M. High-resolution NMR spectroscopy in solids, In: *NMR Basic Principles and Progress*; Diehl, P., Fluck, E., Kosfeld, R., Eds.; Springer-Verlag: Berlin, Germany, 1976, Volume 11.
(21) Rose, M. E. *Elementary theory of angular momentum*; Wiley: New York, 1957.

MA980223Y